11. J. M. Donley, C. A. Sepulveda, P. Konstantinidis, S. Gemballa, R. E. Shadwick, *Nature* **429**, 61–65 (2004).
12. J. B. Graham, K. A. Dickson, in *Tuna: Physiology, Ecology and Evolution*, B. A. Block, E. D. Stevens, Eds. (Academic Press, San Diego, CA, 2001), vol. 19, pp. 121–165.
13. B. A. Block, *J. Morphol.* **190**, 169–189 (1986).
14. F. G. Carey, *Science* **216**, 1327–1329 (1982).
15. R. W. Brill, *Comp. Biochem. Physiol.* **113**, 3–15 (1996).
16. H. A. Shiels, A. Di Maio, S. Thompson, B. A. Block, *Proc. Biol. Sci.* **278**, 18–27 (2011).
17. P. C. Castilho, A. M. Landeira-Fernandez, J. Morrissette, B. A. Block, *Comp. Biochem. Physiol.* **148**, 124–132 (2007).
18. E. D. Stevens, in *Encyclopedia of Fish Physiology: From Genome to Environment*, A. P. Farrell, E. D. Stevens, J. J. Cech, J. G. Richards, Eds. (Academic Press, San Diego, CA, 2011), vol. 2, pp. 1119–1131.
19. R. H. Rosenblatt, G. D. Johnson, *Copeia* **1976**, 367–370 (1976).
20. R. M. Runcie, H. Dewar, D. R. Hawn, L. R. Frank, K. A. Dickson, *J. Exp. Biol.* **212**, 461–470 (2009).
21. J. M. Blank *et al*., *J. Exp. Biol.* **207**, 881–890 (2004).
22. K. C. Weng *et al*., *Science* **310**, 104–106 (2005).
23. J. J. Polovina, D. Hawn, M. Abecassis, *Mar. Biol.* **153**, 257–267 (2008).
24. J. E. Olney, in *Species Identification Guide for Fisheries Purposes. Part 1 (Elopidae to Linophrynidae)*, K. E. Carpenter, V. H. Niem, Eds. (FAO, Rome, 1999), pp. 155–169.
25. J. R. Hyde, K. E. Underkoffler, M. A. Sundberg, *Mol. Ecol. Resour.* **14**, 1239–1247 (2014).
26. J. Childers, S. Snyder, S. Kohin, *Fish. Oceanogr.* **20**, 157–173 (2011).

ACKNOWLEDGMENTS

We thank H. Aryafar, S. Kohin, J. Renfree, R. Vetter, J. Wraith, and the crew of the M/V *Ventura II* for help with opah capture, sampling, tagging, filming, and data visualization. We also thank C. Sepulveda for conversations and D. Bernal, R. Vetter, and R. Runcie for reviewing drafts of the manuscript. S. Snyder provided data from *T. alalunga*. We dedicate this paper to the late Dr. Jeffrey B. Graham, who spent much of his career studying regional endothermy in fishes and would have greatly enjoyed seeing this discovery. Data reported in this paper are archived at DOI: 10.5061/dryad.hq4v0.

SUPPLEMENTARY MATERIALS

www.sciencemag.org/content/348/6236/786/suppl/DC1
Materials and Methods
Figs. S1 and S2
Table S1
References (*27*–*38*)
Movie S1

10 February 2015; accepted 20 April 2015
10.1126/science.aaa8902

NEURODEVELOPMENT

Live imaging of adult neural stem cell behavior in the intact and injured zebrafish brain

Joana S. Barbosa,[1,2] Rosario Sanchez-Gonzalez,[1] Rossella Di Giaimo,[1,3] Emily Violette Baumgart,[1] Fabian J. Theis,[4,5] Magdalena Götz,[1,6,7] Jovica Ninkovic[1,6]*

Adult neural stem cells are the source for restoring injured brain tissue. We used repetitive imaging to follow single stem cells in the intact and injured adult zebrafish telencephalon in vivo and found that neurons are generated by both direct conversions of stem cells into postmitotic neurons and via intermediate progenitors amplifying the neuronal output. We observed an imbalance of direct conversion consuming the stem cells and asymmetric and symmetric self-renewing divisions, leading to depletion of stem cells over time. After brain injury, neuronal progenitors are recruited to the injury site. These progenitors are generated by symmetric divisions that deplete the pool of stem cells, a mode of neurogenesis absent in the intact telencephalon. Our analysis revealed changes in the behavior of stem cells underlying generation of additional neurons during regeneration.

The maintenance of adult neural stem cells (aNSCs) is important for life-long organ homeostasis (*1*) and regeneration (*2*–*4*). There is presently a discrepancy between models describing the behavior of aNSCs in the mammalian brain, one proposing largely depletion of aNSCs (*5*, *6*) and the other some degree of long-term self-renewal (*7*). In the adult zebrafish brain, aNSCs exist not only in a more widespread manner compared with those of mammals but also react to injury by regenerating neurons (*2*, *3*, *8*–*14*). Indeed, the cellular architecture is restored, which includes additional neurogenesis after stab wound injury in the adult zebrafish telencephalon (*2*, *3*, *11*, *13*, *14*). As aNSCs are positioned close to the surface in the zebrafish dorsal telencephalon (*12*, *15*) (Fig. 1A), the behavior of aNSCs in the intact brain and during regeneration of the injured brain can be examined noninvasively by live in vivo imaging.

We established a protocol by which we could follow individual aNSCs over time [fig. S1A and supplementary materials (SM)]. We used the *brassy* zebrafish line, which has low pigment levels, crossed with the *Tg(gfap:GFP)mi2001* transgenic line (*16*), which labeled aNSCs (Fig. 1A). We sparsely labeled the glial fibrillary acidic protein promoter–driven green fluorescent protein (*gfap*:GFP)–positive aNSCs (see SM) by electroporation of plasmids encoding for red fluorescent proteins [tdTomato, mCherry, or red fluorescent protein (RFP)] (fig. S1 and SM). Most of the labeled cells with radial morphology were immunoreactive to GFAP (106 of 124 cells; 85%) (fig. S1, E and F) and did not differ with regard to their proliferation from the overall *gfap*:GFP–positive aNSCs (fig. S1, C and D). Individual tdTomato-labeled NSCs at the dorsal brain surface were identified by their position relative to the stable *gfap*:GFP–positive cells (colored dots in Fig. 1C). These individual cells were then followed by imaging through the thinned skull for a period of 1 month (fig. S1A). As many reporter-positive cells neither moved nor divided, we used their distribution pattern in post-imaging immunostaining and microscopy to re-identify and confirm cell identity of imaged cells (figs. S2, S4, and S5).

In the intact brain, aNSCs rarely divide (*17*, *18*). Indeed, 66 of 109 (61%) of the labeled aNSCs in the intact zebrafish telencephalon stayed quiescent without changing their identity throughout the imaging time (fig. S2), and only 1 of 109 cells followed by live imaging died. However, 14 aNSCs (13%, n = 109) divided during this time. We found that the aNSCs rarely divided symmetrically (1 cell of 109; 0.9%) (Fig. 1C; fig. S3, B and E; fig. S4; and movies S1 and S2), with one aNSC generating two aNSCs, both of which retained *gfap*:GFP expression and the characteristic thick radial process (fig. S4). In contrast, 13 of 14 dividing aNSCs (~93%) divided asymmetrically, generating one cell with aNSC identity (radial morphology and *gfap*:GFP expression) and one cell that lacked the radial morphology (Fig. 2; fig. S3, B and E; figs. S5 and S6; and movies S3 and S4). Of these progeny lacking radial morphology, 25% (two of eight cells) also lost *gfap*:GFP expression (GFP-negative progeny in fig. S3, B and D). Because GFP is very stable, the protein can persist even after the cell is no longer an aNSC (Fig. 1B), and some GFP-positive cells do not express aNSC markers (*15*). Although asymmetrically generated daughter cells differ in regard to inheritance of GFP, all of them lose the radial glia morphology, the defining criteria for the asymmetric divisions (93%, 13 of 14 dividing aNSCs). Some cells that had lost the radial process, however, were not immunoreactive for the neuronal marker HuC/D (figs. S3B and S5C), which implies that they may be intermediate progenitor cells.

To examine the behavior of Sox2-positive intermediate progenitors (fig. S7), we used Moloney murine leukemia virus–based retroviral vectors to stably transduce progenitor cells (*18*). We analyzed their clonal progeny that contained no glia

[1]Institute of Stem Cell Research, Helmholtz Center Munich, Munich, Germany. [2]Ph.D. Program in Biomedicine and Experimental Biology (BEB), Center for Neuroscience and Cell Biology, University of Coimbra, Coimbra, Portugal. [3]Department of Biology, University of Naples Federico II, Naples, Italy. [4]Institute of Computational Biology, Helmholtz Center Munich, Munich, Germany. [5]Institute for Mathematical Sciences, Technical University Munich, Garching, Germany. [6]Biomedical Center, University of Munich, Munich, Germany. [7]Munich Cluster for Systems Neurology "SyNergy," Ludwig Maximilian University of Munich, Munich, Germany.
***Corresponding author. E-mail: ninkovic@helmholtz-muenchen.de**

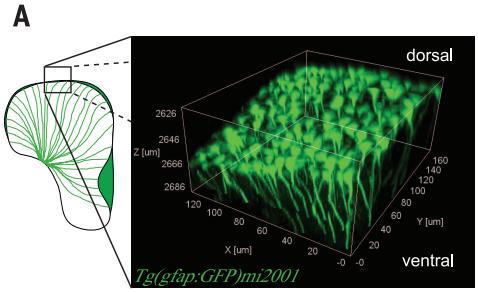

B

	Cell classification	aNSC	Non-glial cells	
live imaging	morphology	radial	non-radial	non-radial
	Tg(gfap:GFP)	+	+/-	-
	Tg(HuC:GFP)	-	-	+
immunohistochemistry	GFAP	+	-	-
	HuCD	-	-	+
	Sox2	+	+	-
	Cell identity	aNSC	IP	neuron

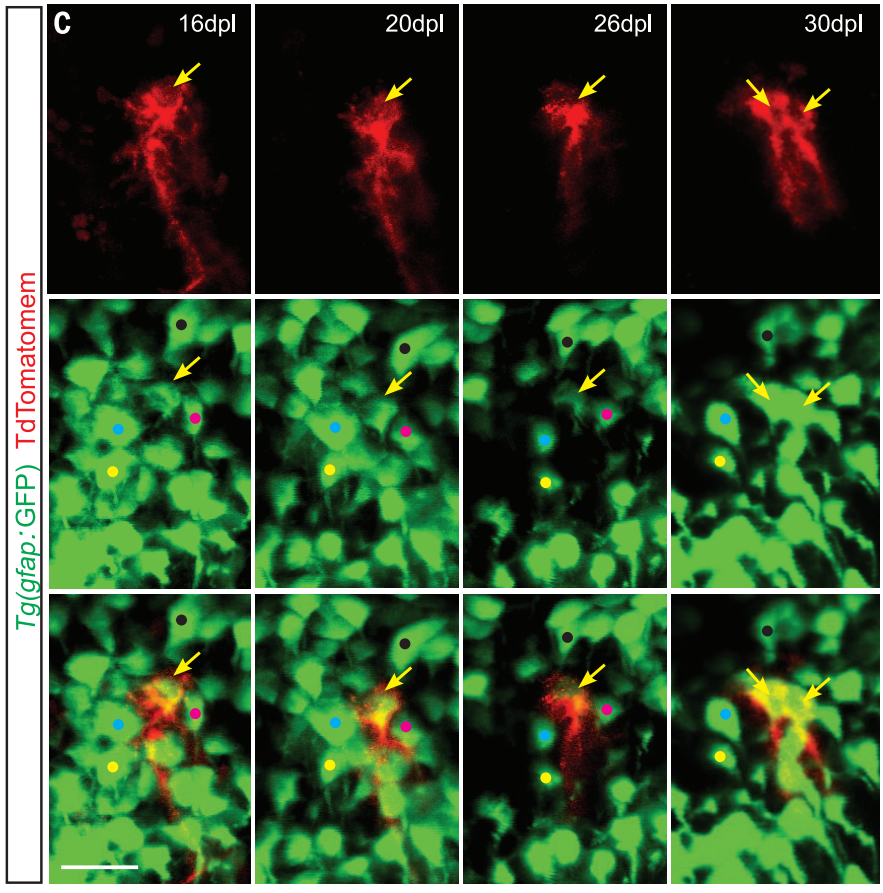

Fig. 1. In vivo imaging of aNSCs in the intact brain. (**A**) Scheme of a telencephalic hemisection with the ventricular zone, containing aNSCs (green), and the parenchyma (white), which is mostly composed of neurons. (Right) A three-dimensional view of aNSCs in the telencephalon of a live adult *Tg(gfap:GFP)mi2001* zebrafish. (**B**) Summary of the criteria used to classify different types of cells. (**C**) Confocal images of the same tdTomato-labeled aNSC in the *Tg(gfap:GFP)mi2001* transgenic line at different time points depicting its symmetric gliogenic (RG) division generating two aNSCs [30 days post labeling (dpl)]. (See also fig. S4 for all time points imaged.) Yellow arrows point to single cells. Scale bar, 20 μm. Abbreviation: IP, intermediate progenitors.

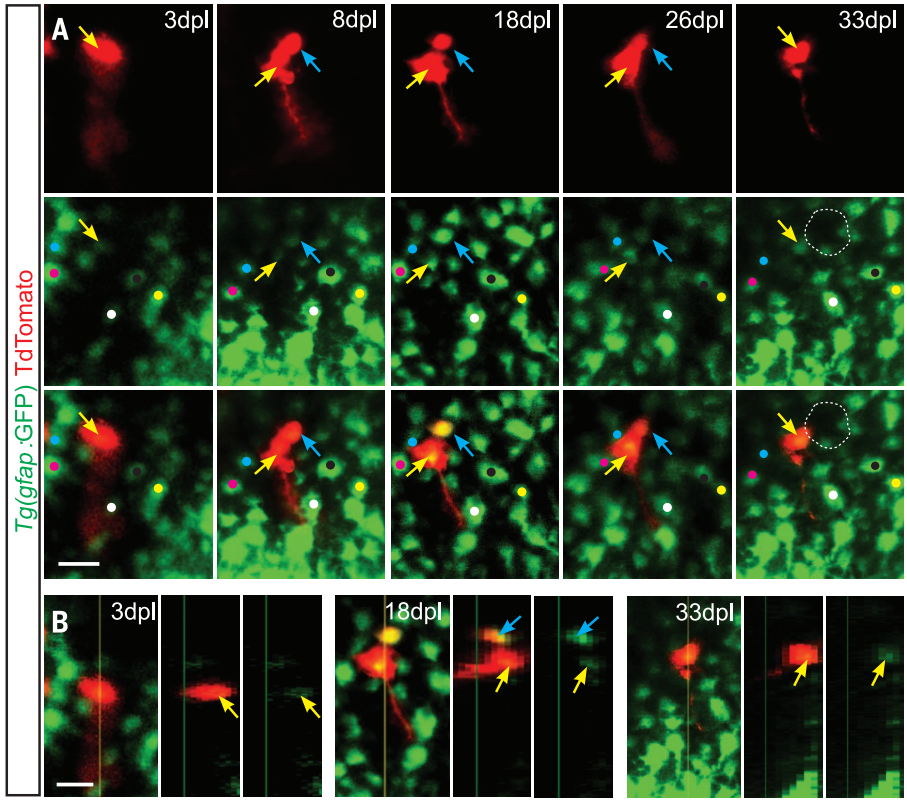

Fig. 2. Asymmetric division of an aNSC in the adult telencephalon. (**A**) Confocal images of the same tdTomato-labeled aNSC in the *Tg(gfap:GFP)mi2001* transgenic line at different time points depicting its asymmetric division producing one aNSC (yellow arrow) and one intermediate progenitor (8 dpl, blue arrow). (**B**) Orthogonal projections through the Z-stack. Scale bar, 20 μm.

and therefore likely originated from the intermediate progenitors. The mean size of the clone was 3.9 cells, which indicated some degree of amplification in the lineages generated by intermediate progenitors (fig. S7). Among the amplifying clones (≥2 cells) 44% (four of nine clones) were HuC/D-positive cells only (fig. S7) (maximal clone size of pure neuronal clones was eight cells). We conclude that the number of neurons generated by a stem cell can be enlarged by intermediate progenitors.

Besides asymmetric division, we also found that 17% (19 of 109 cells) of the observed stem cells lost their aNSC hallmarks and up-regulated HuC/D (Fig. 3, A to D, and fig. S8), which is a representative neuronal marker (fig. S9, A and B) that is detected either by HuC/D immunostaining in postimaging analysis (Fig. 3, C and D) or GFP expression in the *Tg(HuC:GFP)* transgenic line in live imaging (fig. S9, C to E). These observations suggest that some aNSCs convert directly into neurons without division [for all the lineages that show direct conversion, see (fig. S3, A and C)]. We cannot exclude that NSCs may have divided before our observation period. However, we found examples of aNSCs converting into neurons without division within more than 2 weeks of imaging time (fig. S3, A and C), which suggests that such a division must have occurred some time before [for an example of direct conversion at very early embryonic stages see (*19*)]. Taken together, during our observation period of several weeks, aNSCs generated neurons in a self-consuming mode (direct conversion) and a self-maintaining mode (asymmetric division) in the intact brain.

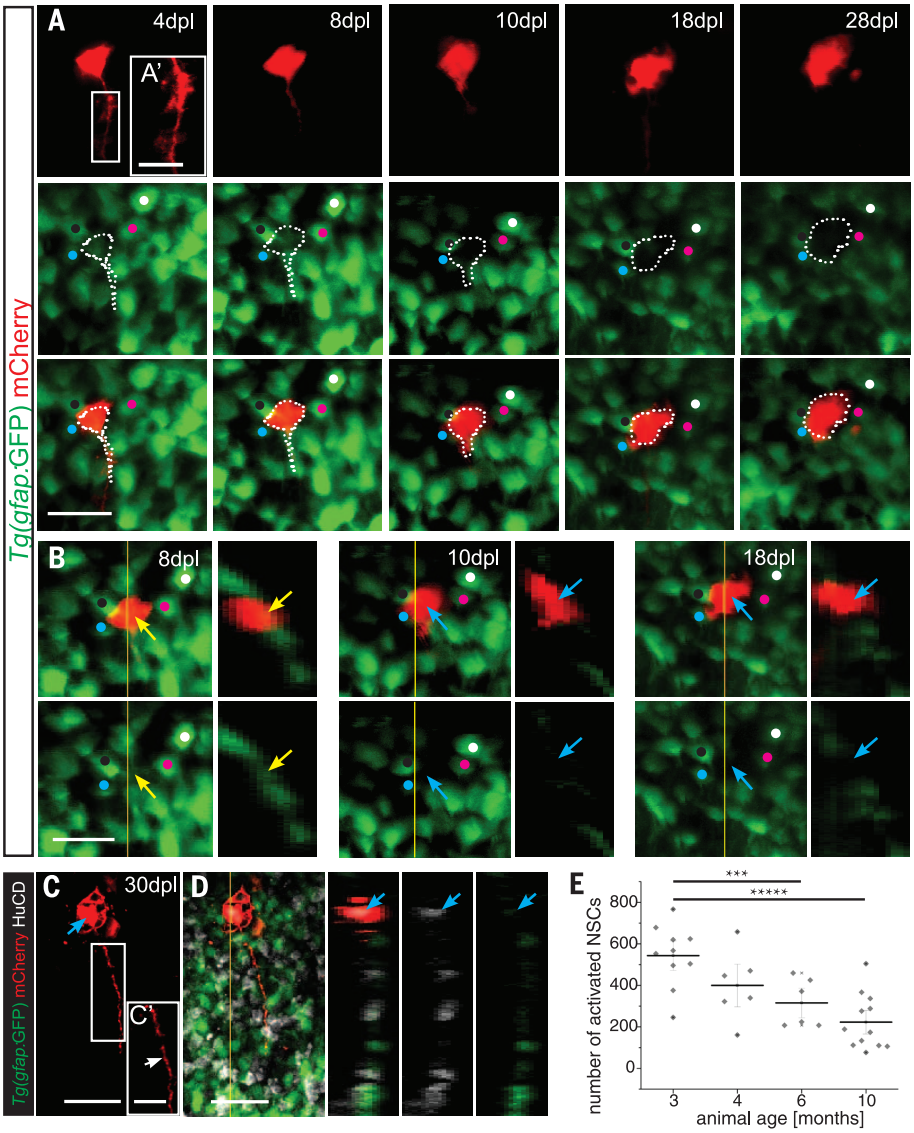

Fig. 3. aNSCs directly convert into neurons in the intact zebrafish telencephalon. (**A** and **B**) Confocal images with orthogonal projections (B) of the same mCherry-labeled aNSC in the *Tg(gfap:GFP)mi2001* line at different time points, depicting the conversion of a *gfap*:GFP–positive aNSC with radial morphology [4 dpl, yellow arrow in (B)] to a *gfap*:GFP–negative cell without the radial morphology [28 dpl, blue arrow in (B)] (See also fig. S8 for all time points.) (**C** and **D**) Immunostainings at 30 dpl for GFP, mCherry, and HuC/D in whole-brain samples with orthogonal projections (D) confirming the neuronal (HuC/D$^+$) identity of the imaged cell (blue arrows). Note the thicker, ramified typical RG process in (**A'**) in contrast to the thinner neuronal process in (**C'**), only observed after staining. (**E**) The number of activated aNSCs determined by FACS in the dorsal telencephalon of animals at different ages. Dots represent single animals and lines the mean ± SEM for the single age. ***$P < 0.005$; *****$P < 0.0001$ (Mann-Whitney test). Scale bars: (A) to (D), 20 μm; (A') and (C'), 10 μm.

The stem cell pool is sustained by the mode of division in which 12% (13 of 109 cells) of aNSCs divide asymmetrically to generate another stem cell and a neuronal progenitor or neuron. The stem cell pool is only rarely added to by less than 1% (1 of 109 cells) of aNSCs undergoing symmetric divisions and depleted by self-consuming direct conversion [19 of 109 aNCSs (17%)]. As this behavior would predict a gradual net loss of NSCs, we determined the number of activated, proliferating cell nuclear antigen–positive aNSCs (Fig. 3E, fig. S10, and SM) at different ages using fluorescence-activated cell sorting (FACS) (Fig. 3E, fig. S10, and table S2). The number of aNSCs significantly decreased in 6 and 10 months compared with the number in 3-month-old fish (Fig. 3E and table S2), in agreement with the prediction based on the live imaging. Taken together, both live imaging and FACS analysis demonstrate the gradual net decrease of activated aNSC numbers (Fig. 3E and SM). This decrease parallels observations of decline in neurogenesis with age in zebrafish (*20*).

We then asked how the various modes of stem cell behavior may support the increased neurogenesis after stab wound injury in the telencephalic parenchyma (*2*, *3*, *13*). To follow aNSCs after injury, we labeled them by electroporation as described above, 4 to 8 days before the injury to allow the fluorescence protein to rise to levels sufficient for detection before the first imaging session. We imaged the aNSCs and their progeny using the same procedures as for the intact brain (fig. S1A). We found that proliferation of aNSCs increased twofold after injury [from 13% to 26% (8 of 31 aNSCs), $P = 0.07$] (Fig. 4B) in agreement with the increased number of proliferating aNSCs after injury previously observed at the population level (*2*, *3*, *11*). No single stem cell divided more than once in response to injury (fig. S3, B and D). Thus, the additional neurogenesis in response to injury is due to recruitment of quiescent aNSCs. Indeed, tracing aNSCs at the clonal level by using lipofection (fig. S11) fully supported the in vivo imaging data, as we detected a larger number of clones that underwent proliferation [two cell clones (fig. S11I)], but we did not observe an increase in the number of clones larger than two cells in response to injury. The recruited stem cells were not susceptible to cell death, as we observed fewer than 1% of cells with the morphological changes of dying cells in both intact and injured telencephalon (fig. S12A), and we found no increase in terminal deoxynucleotidyl transferase–mediated

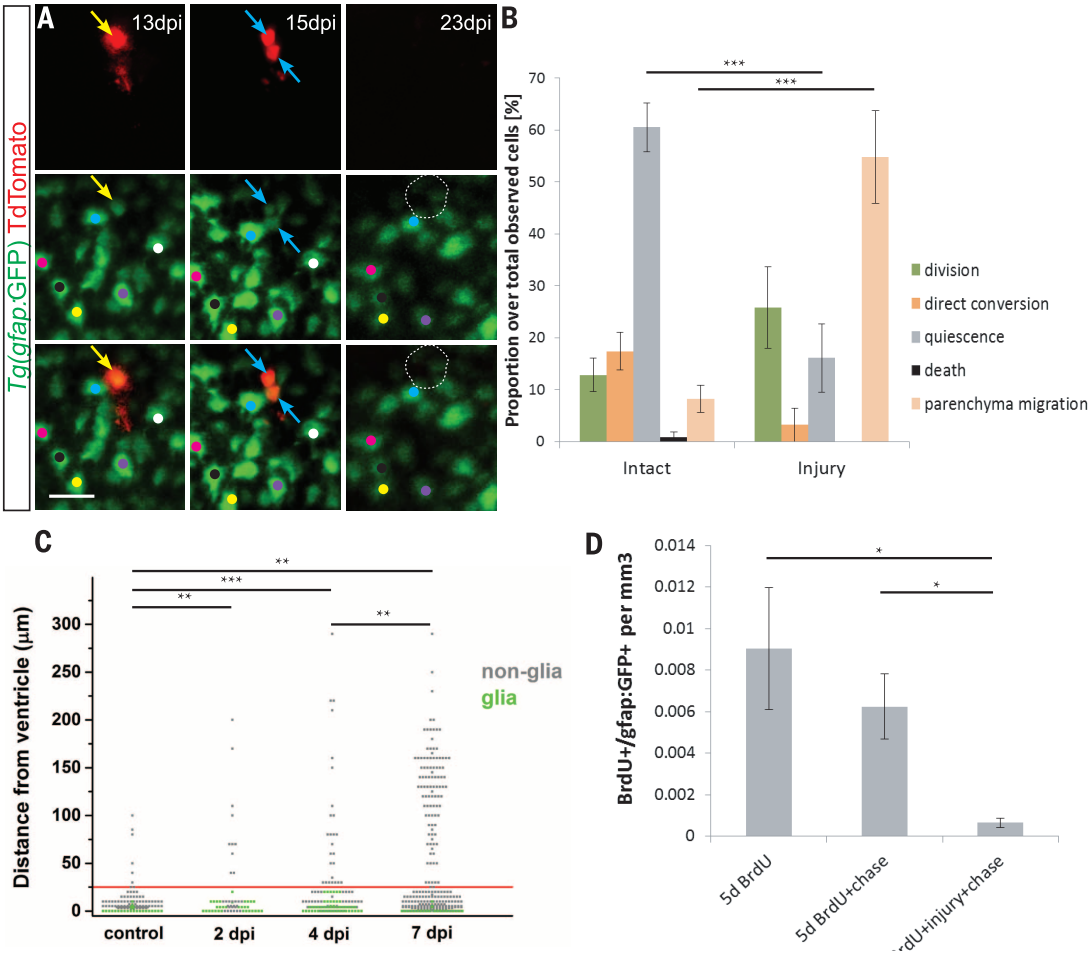

Fig. 4. Behavior of aNSCs after injury. (**A**) Confocal images of the same tdTomato-labeled aNSC (yellow arrow) in the *Tg(gfap:GFP)mi2001* transgenic line at different time points, depicting its symmetric division producing two non-RG cells [15 days post injury (dpi), blue arrows] (See also fig. S13 for all time points.) (**B**) The abundance of different aNSC behaviors in the control and injured telencephalon based on the live, single-cell in vivo imaging. $*P < 0.05$, $***P < 0.001$ (one-sided Fisher's exact test). (**C**) The distance from the ventricular surface of electroporated cells generated from the aNSCs in the intact and injured brain. Red line marks the zone of adult constitutive neurogenesis. (**D**) The number of aNSCs 1.5 months after their labeling with the DNA base analog BrdU in the control and injured brain. Note the significant decline after injury. (C) and (D) $*P < 0.05$, $**P < 0.01$, $***P < 0.001$ (Mann-Whitney test).

deoxyuridine triphosphate nick end labeling (TUNEL)–positive cells at the dorsal telencephalon surface either in aNSCs or their progeny after injury (fig. S12, C to I).

Next, we used live imaging to compare the mode of cell division after injury to the one observed in the healthy control brain. Asymmetric aNSC divisions remained the predominant mode of division even after injury [75% of all dividing aNSCs (6 of 8 divisions) compared with 93% (13 of 14 divisions) in the control brain] (fig. S3, D and E). In addition, we also observed symmetric divisions, but in contrast to the control brains, these were not maintaining aNSCs but generated two cells that lost the aNSC hallmarks [25% of all dividing aNSCs after injury (two of eight divisions)] (Fig. 4A and figs. S3E and S13). This mode of division, consuming NSCs for the generation of two intermediate progenitors—that then disappear from the aNSC layer (Fig. 4A) and migrate toward the injury (Fig. 4C)—appeared to be a special mode triggered by the injury, as we did not observe this type of division in the control brain (fig. S3E). The clonal analysis of aNSC progeny further corroborated this change in the cell division mode, as we could observe a twofold increase in the proportion of intermediate progenitor or neuronal clones containing two or more cells after injury (nonglial clones in fig. S14).

The increase in neuronal output via intermediate progenitors was coincident with the 55% (17 of 31 cells) of all labeled aNSCs migrating into the parenchyma that could no longer be followed by live imaging after injury (Fig. 4B and fig. S15A). With brains fixed and sectioned after electroporation (fig. S15, C to G), we observed a gradual increase in the number of labeled cells deep within the injured brain parenchyma (Fig. 4C). These were HuC/D-positive neurons (fig. S15, F and G). Likewise, when intermediate progenitors were labeled by retroviral vectors and brains were fixed and stained 14 days after injury, many of their derivatives had become HuC/D-positive neurons that migrated toward the injury site in the parenchyma (fig. S15, H to K). Increased consumption of aNSCs (migration to parenchyma, symmetric nongliogenic division, and direct conversion) in the injured brain compared with the control (Fig. 4B) suggests even faster depletion of aNSCs after injury. Indeed, we observed a significantly lower number of label-retaining aNSCs by immunostaining (see SM) in brains 6 weeks after injury compared with the controls (Fig. 4D and fig. S16). These data therefore suggest that changes in neurogenesis contribute to the response to injury: Fewer stem cells remain quiescent [16% (5 of 31 cells) NSCs in the injured brain versus 61% (66 of 109 cells) in the intact brain] (Fig. 4B), and a pathway is added by which symmetric NSC division generates two intermediate progenitors that then give rise to a larger neuronal progeny (fig. S17).

Here, we show how aNSCs generate neurons in a manner that depletes the stem cell pool slowly with age, similar to the clonal aNSC behavior in the mouse subependymal zone, which leads to generating a discrete cohort of neurons and depleting itself (*6*). This depletion is further rapidly increased after injury in the zebrafish brain, as shown here by live imaging and immunostaining. Thus, the increase in neurogenesis after injury comes at the expense of depletion of aNSCs, perhaps drawing on quiescent NSCs. Therefore, the maintenance of aNSCs seems to be the key for long-term regeneration, and our data lay the basis for understanding the molecular pathways regulating NSC behavior involved in the regeneration process.

REFERENCES AND NOTES

1. I. Imayoshi *et al.*, *Nat. Neurosci.* **11**, 1153–1161 (2008).
2. E. V. Baumgart, J. S. Barbosa, L. Bally-Cuif, M. Götz, J. Ninkovic, *Glia* **60**, 343–357 (2012).
3. V. Kroehne, D. Freudenreich, S. Hans, J. Kaslin, M. Brand, *Development* **138**, 4831–4841 (2011).
4. L. Mchedlishvili *et al.*, *Proc. Natl. Acad. Sci. U.S.A.* **109**, E2258–E2266 (2012).
5. J. M. Encinas *et al.*, *Cell Stem Cell* **8**, 566–579 (2011).
6. F. Calzolari *et al.*, *Nat. Neurosci.* **18**, 490–492 (2015).

7. M. A. Bonaguidi *et al.*, *Cell* **145**, 1142–1155 (2011).
8. M. M. Reimer *et al.*, *J. Neurosci.* **28**, 8510–8516 (2008).
9. M. Carlén *et al.*, *Nat. Neurosci.* **12**, 259–267 (2009).
10. K. Meletis *et al.*, *PLOS Biol.* **6**, e182 (2008).
11. M. März, R. Schmidt, S. Rastegar, U. Strähle, *Dev. Dyn.* **240**, 2221–2231 (2011).
12. B. Adolf *et al.*, *Dev. Biol.* **295**, 278–293 (2006).
13. B. Ayari, K. H. El Hachimi, C. Yanicostas, A. Landoulsi, N. Soussi-Yanicostas, *J. Neurotrauma* **27**, 959–972 (2010).
14. N. Kishimoto, K. Shimizu, K. Sawamoto, *Dis. Model. Mech.* **5**, 200–209 (2012).
15. M. März *et al.*, *Glia* **58**, 870–888 (2010).
16. R. L. Bernardos, P. A. Raymond, *Gene Expr. Patterns* **6**, 1007–1013 (2006).
17. P. Chapouton *et al.*, *J. Neurosci.* **30**, 7961–7974 (2010).
18. I. Rothenaigner *et al.*, *Development* **138**, 1459–1469 (2011).
19. J. E. Bestman, J. Lee-Osbourne, H. T. Cline, *J. Comp. Neurol.* **520**, 401–433 (2012).
20. K. Edelmann *et al.*, *J. Comp. Neurol.* **521**, 3099–3115 (2013).

ACKNOWLEDGMENTS

We thank P. Raymonds for sharing the *Tg(gfap:GFP)mi2001* fish line. We also thank T. Özturk, A. Steiner-Mazzardi, and S. Hübinger for excellent technical help; A. Lepier for the viral vector production; S. Hake for the help with intracellular FACS; and P. Alexandre, V. Borrell, P. Chapouton, L. Dimou, and L. Godinho for critical reading of the manuscript. We acknowledge funding to J.N. from the German Research foundation (DFG) by the Sonderforschungsbereich (SFB) 870 and Schwerpunktprogramm "Integrative analysis of olfaction"; to M.G. from the DFG by the SFB 870, the Leibniz Prize, the Helmholtz Alliance ICEMED, and the European Research Council grant ChroNeuroRepair: Grant Agreement no. 340793; and to J.S.B. from the Fundação para a Ciência e Tecnologia, Portugal (FCT); to F.T. from European Research Council grant LatentCauses and a BioSysNet grant by the Bavarian ministry of education and research. Supplementary materials contain additional data.

SUPPLEMENTARY MATERIALS

www.sciencemag.org/content/348/6236/789/suppl/DC1
Materials and Methods
Figs. S1 to S17
Tables S1 and S2
References (*21*–*26*)
Movies S1 to S4

12 November 2014; accepted 15 April 2015
10.1126/science.aaa2729

ARCHAEOLOGY

The makers of the Protoaurignacian and implications for Neandertal extinction

S. Benazzi,[1,2]* V. Slon,[3] S. Talamo,[2] F. Negrino,[4] M. Peresani,[5] S. E. Bailey,[2,6] S. Sawyer,[3] D. Panetta,[7] G. Vicino,[8] E. Starnini,[9,10] M. A. Mannino,[2] P. A. Salvadori,[7] M. Meyer,[3] S. Pääbo,[3] J.-J. Hublin[2]

The Protoaurignacian culture is pivotal to the debate about the timing of the arrival of modern humans in western Europe and the demise of Neandertals. However, which group is responsible for this culture remains uncertain. We investigated dental remains associated with the Protoaurignacian. The lower deciduous incisor from Riparo Bombrini is modern human, based on its morphology. The upper deciduous incisor from Grotta di Fumane contains ancient mitochondrial DNA of a modern human type. These teeth are the oldest human remains in an Aurignacian-related archaeological context, confirming that by 41,000 calendar years before the present, modern humans bearing Protoaurignacian culture spread into southern Europe. Because the last Neandertals date to 41,030 to 39,260 calendar years before the present, we suggest that the Protoaurignacian triggered the demise of Neandertals in this area.

The timing and pattern of the biological and cultural shifts that occurred in Western Europe around 45,000 to 35,000 calendar years before the present (cal yr B.P.) fuel continuing debates among paleoanthropologists and prehistorians (*1*–*3*). During this period, Neandertals were replaced by anatomically modern humans (AMHs) (*4*), and a variety of "transitional" and early Upper Paleolithic cultures emerged. Among them, the Protoaurignacian is crucial to current interpretations regarding the timing of arrival of AMHs and their interaction with Neandertals (*5*–*9*).

The Protoaurignacian appeared around 42,000 cal yr B.P. (*8*, *10*) in southwest and south-central Europe (fig. S1). In addition to the presence of personal ornaments, such as perforated shells and worked bones, the Protoaurignacian is characterized by a dominance of bladelets with typical retouched standardized implements such as Font-Yves points and Dufour bladelets produced from unipolar cores (*5*). This techno-complex has been tentatively linked to the Ahmarian industry of the Levant (*6*, *9*). Because the Ahmarian has been attributed to modern humans (*11*), it has been suggested that the Protoaurignacian reflects a westward population movement of AMHs from the Near East (*1*, *7*). However, because only three nondiagnostic human remains are associated with this culture, it is still uncertain who the makers of the Protoaurignacian were (*9*, *12*). The fossil remains associated with the Protoaurignacian that are available for study consist of the undiagnostic skeletal fragments of a fetus retrieved from Le Piage rock shelter (France) (*13*), for which the stratigraphic integrity of the Châtelperronian/Aurignacian sequence has been questioned (*5*), and two deciduous incisors from two northern

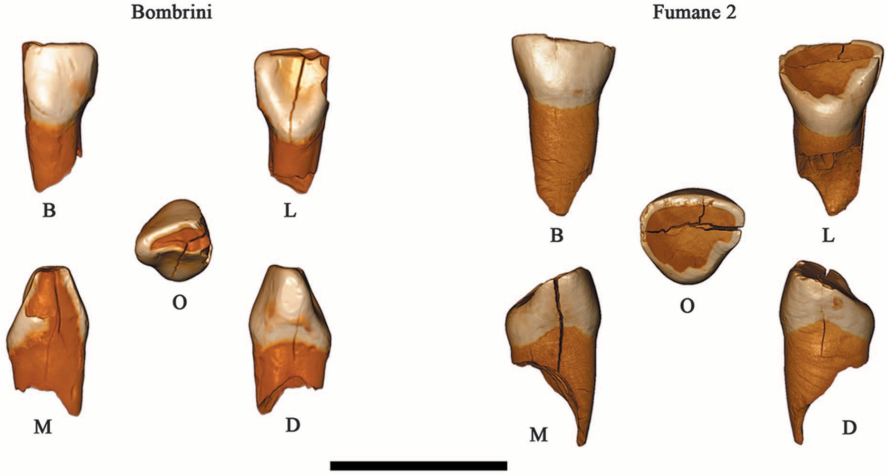

Fig. 1. Three-dimensional digital models of the Protoaurignacian human remains. The Bombrini tooth is a lower left lateral deciduous incisor (Ldi_2), whereas Fumane 2 is an upper right lateral deciduous incisor (Rdi^2). B, buccal; D, distal; L, lingual; M, mesial; O, occlusal. Scale bar, 1 cm.

[1]Department of Cultural Heritage, University of Bologna, Via degli Ariani 1, 48121 Ravenna, Italy. [2]Department of Human Evolution, Max Planck Institute for Evolutionary Anthropology, Deutscher Platz 6, 04103 Leipzig, Germany. [3]Department of Evolutionary Genetics, Max Planck Institute for Evolutionary Anthropology, Deutscher Platz 6, 04103 Leipzig, Germany. [4]Dipartimento di Antichità, Filosofia, Storia e Geografia, Università di Genova, Via Balbi 2, 16126 Genova, Italy. [5]Sezione di Scienze Preistoriche e Antropologiche, Dipartimento di Studi Umanistici, Corso Ercole I d'Este 32, Università di Ferrara, 44100 Ferrara, Italy. [6]Center for the Study of Human Origins, Department of Anthropology, New York University, 25 Waverly Place, New York, NY 10003, USA. [7]CNR Institute of Clinical Physiology, National Research Council, Via G. Moruzzi 1, 56124 Pisa, Italy. [8]Museo Archeologico del Finale, Chiostri di Santa Caterina, 17024 Finale Ligure Borgo, Italy. [9]Scuola di Scienze Umanistiche, Dipartimento di Studi Storici, Università di Torino, via S. Ottavio 20, 10124 Torino, Italy. [10]Museo Preistorico Nazionale dei Balzi Rossi, Via Balzi Rossi 9, 18039 Ventimiglia, Italy.
***Corresponding author. E-mail: stefano.benazzi@unibo.it**